Scientific Research Publishing

Atmospheric and Climate Sciences, 2021, 11, 373-397
https://www.scirp.org/journal/acs
ISSN Online: 2160-0422
ISSN Print: 2160-0414

Convective Rainfall in Lake Victoria Watershed and Adjacent Equatorial Africa

Felipe Vemado, Augusto José Pereira Filho

Departmento de Ciências Atmosféricas, Instituto de Astronomia, Geofísica e Ciências Atmosféricas, Universidade de São Paulo, São Paulo, Brazil
Email: fvfelp@gmail.com, augusto.pereira@iag.usp.br

How to cite this paper: Vemado, F. and Filho, A.J.P. (2021) Convective Rainfall in Lake Victoria Watershed and Adjacent Equatorial Africa. *Atmospheric and Climate Sciences*, **11**, 373-397.
https://doi.org/10.4236/acs.2021.113022

Received: March 30, 2021
Accepted: May 16, 2021
Published: May 19, 2021

Abstract

An integrated satellite precipitation estimation dataset, namely, the Climate Prediction Center morphing method (CMORPH), was used to analyze precipitation regimes across Equatorial Africa between 3˚S - 1˚N and 24˚E - 42˚E from 2000 to 2014. This region includes the Rift Valley, part of the Congo Forest, and the Lake Victoria (LV) basin, the second largest lake in the area of the world. Hovmöller diagrams were obtained for all organized convective systems to estimate their spans, duration, and phase speeds. The analysis included 33,189 episodes of westward propagating convective systems. Within the study area, lake and land breezes tend to trigger convection and precipitation over LV as well as mountain-valley circulation trigger thunderstorms over the mountains east of LV and western Rift Valley. The statistics of convective systems streaks on longitude-time diagrams were obtained for yearly frequencies of starting and ending longitudes and times among other morphologic variables. Results indicate organized precipitation episodes tend to move westward across Rift valley and Congo forest with an average phase speed of 10.3 $m \cdot s^{-1}$. More than 50% of them are triggered over LV and propagate more than 600 km at an average phase speed of 12.1 $m \cdot s^{-1}$. These convective systems tend to produce high rainfall rates hundreds of kilometers away into the Congo Forest. Half of all episodes of organized convection analyzed have phase speeds between 8 $m \cdot s^{-1}$ and 16 $m \cdot s^{-1}$, lasting 8 hr to 16 hr. Most precipitating systems start east of LV and west of Rift Valley in the afternoon to early morning and propagates less than 400 km. Finally, hourly precipitation accumulation and lightning density analysis indicate three preferable regions for convective initiation: 1) The mountain range east of LV; 2) Midwest of LV, and; 3) The Congo Forest mountain range.

Keywords

Lake Victory, Precipitation, Deep Convection, Diurnal Cycle, CMORPH

1. Introduction

Precipitation estimation from integrating passive microwave (PMW) and IR sensors onboard geostationary and polar orbit satellites is an important data source to study deep convection in tropical areas where rain gauges and weather radar measurements are sparse. This work analyzes the spatial-temporal evolution of precipitating systems in Equatorial Africa with satellite rainfall estimates of the Climate Prediction Center morphing method—CMORPH as in [1]. This method is based on PMW and IR measurements with an 8-km and half-hour time-spatial resolution. It has been successfully used in several studies in South America by [2]-[7]. In the present study, CMORPH datasets are used to analyze the diurnal cycle of convection and respective dynamic and thermodynamic footprints from the Rift Valley to the Congo Forest with an emphasis on the mesoscale system induced by the lake and mountain-valley circulations by Lake Victory and the Easterlies.

Lake Victoria (LV) is the second-largest freshwater lake on the planet (**Figure 1(a)**) about 400 km long (north-south) and 250 km wide (west-east) covering an area of 68,800 km^2 with an average lake depth of 40 m. So, the LV area is large enough to impact the local climate [8]. LV watershed outlet is at White Nilo near Jinja and Uganda and is composed of 17 tributaries. The main tributary is the Kagera River according to [9]. [10] estimated that the total water volume of LV is composed of streamflow contributions from tributaries (20%) and direct precipitation over LV (80%).

Fishing, transportation, and tourism are the main socio-economic activities of LV. These activities are hindered and highly affected by severe thunderstorms that form over LV between late afternoon and early morning. These supercells yield high rainfall rates, wind gusts, and lake waves that claim the lives of thousands of people every year according to local authorities. The National Lake Rescue Institute indicates that LV is the region with the highest death toll per square kilometer of the planet.

According to [11], the spatial maximum lightning flash density estimated from the Wide Lightning Location Network (WWLLN) database is centered at 2˚S and 28˚E over Congo Forest in equatorial Africa. Their results also indicate a lower secondary maximum eastward over LV in most years between 2005 and 2013. There are few studies on the diurnal cycle of LV thunderstorms. [12] Chamberlain *et al.* (2013) analyzed cloud fraction frequencies of IR brightness temperatures < 210 K at a 3-hr time interval and found a maximum cloud fraction northwest of LV in the early morning and east of LV in the late afternoon. [13] performed the 150-year Hadley Centre regional model HadRM3P simulation runs over Lake Victoria. Simulations reproduced a lake-land breeze circulation with maximum precipitation over LV with a positive bias. They recommended using higher resolution runs coupled with two-way interaction between LV and its surroundings to improve the accuracy of lake surface temperature (LST).

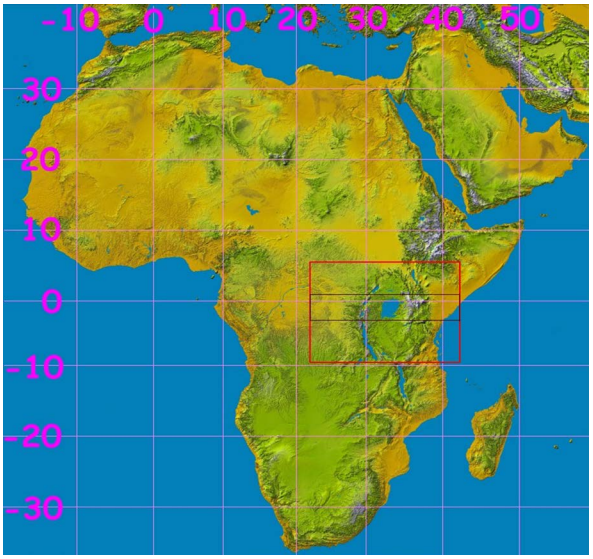

(a)

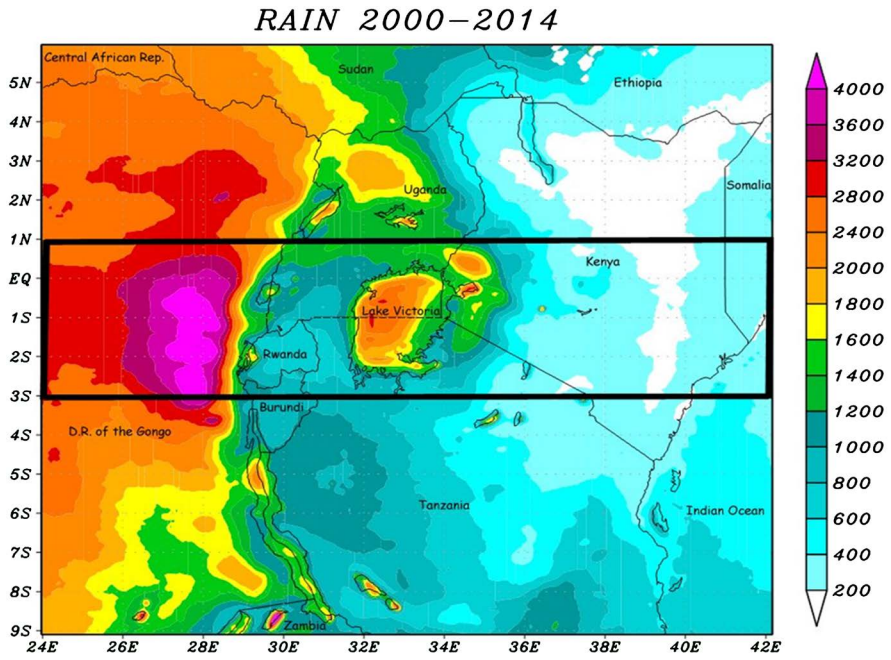

(b)

Figure 1. Topographic map of Africa adapted from NASA/JPL/NIMA (a) and yearly CMORPH precipitation average field (mm) between 2000 and 2014 (b). Red and black rectangles show CMORPH and time-longitude areas, respectively. Longitudes, latitudes, countries, geographic contours, and color scale are indicated. Bodies of water and mountains in (a) in blue and greyscale, respectively. Source (a): https://photojournal.jpl.nasa.gov/catalog/PIA04965.

[10] and [14] correlated satellite IR data with rain gauges to estimate precipitation over LV between 1956 and 1978 and they both obtaining similar spatial distribution patterns. [14] indicated inflows and outflows from tributaries of LV watershed are much less than evaporation and precipitation over LV.

Mesoscale convective systems over Central Africa propagate westward hun-

dreds of kilometers as the ones in Amazonian analyzed by [3]. Some are embedded in eastward-propagating Kelvin wave trains. According to [15], these systems have a large interannual variability. High (low) Kelvin wave activity over Africa tends to occur during dry (wet) years. [16] indicates that their phase speeds decrease from 24 $m \cdot s^{-1}$ in the Pacific and western Atlantic to 14 $m \cdot s^{-1}$ in tropical Africa. Kelvin wave patterns are not usual in Hovmöller diagrams. So, this work analysis all westward propagating systems, the majority of the precipitating episodes.

The diurnal cycle of convective systems, their frequencies, phase speeds, spans, and duration over the highest convective part of Congo Forest and Rift Valley are studied with CMORPH hourly-rainfall estimates between January 2000 and December 2014 and Hovmöller time-longitude diagrams between 3˚S to 1˚N (**Figure 1(a)**). Hovmöller diagrams were used to estimate the starting longitude of the precipitating systems, their duration, and span. They were also useful to infer the underlying dynamics and thermodynamics of mesoscale convective systems.

CMORPH is one of the most complete, longest, and highest resolution datasets available to study spatial-temporal features of deep convection over Equatorial Africa. This research focuses on deep convection in the LV region and interactions with easterlies and downstream impacts in Congo Forest. This study analyzes daily, monthly, and yearly CMORPH spatial patterns of rainfall accumulation in Equatorial Africa and respective lighting imaging sensor (LIS) data onboard the EOS TRMM satellite. The latter records the time and location of a flash at 0.1˚ spatial resolution with high detection efficiency [17]. Indeed, the Congo region has one of the highest concentrations of lightning strikes on Earth according to [11] though there is another local high lightning strike concentration.

[18] showed even small areas as Wheeler Lake in northern Alabama influences the local climate. They studied mesoscale circulation induced by the lake. Lake breezes were highly sensitive to the synoptic circulation that produced complex circulation and changed rainfall patterns, humidity, and solar irradiance. Furthermore, [19] showed lakes with a diameter > 100 km induced sea-breeze-like lake-breeze circulation. Wind speeds inland extent and the depth of lake breezes tend to decrease with the decrease of lake diameter (25 km to 10 km). Moreover, the sensitivity of these variables is highest in the afternoon through mid to late morning. Lakes smaller than 10 km have no significant effects on local circulation. The depth of lake-breeze is insensitive to lake size when heat fluxes are low and environmental stability is high according to [19] and [20]. The LV breeze is similar to a sea breeze given its large area, independently of the thermodynamic stability and heat fluxes. Its impact inland is highest between dawn to early morning. This direct circulation triggers thunderstorms interacting with eastward propagating weather systems as seen in Section 3.

[21] studied Great Lakes breezes and observed convection along the lake-breeze

fronts and severe thunderstorms, occasionally. [22] conducted numerical simulations of an idealized lake shape and preferred convergence and divergence regions for different wind conditions to explain snowfall and rainfall patterns over the Great Lakes region, much higher downstream from lakes due to the high gradient between the lake and air temperature, especially in winter. [23] observed a similar precipitation lake effect over Lake Champlain in Vermont, USA. [24] studied topography effects on lake-breeze in Salt Lake Valley that intensified the lake-breeze with 600 m to 800 m deep boundary layers. [25] observed the same effect in the Itaipú lake region, Paraná, Brazil, with an upslope topography intensifying lake-breeze with divergence over the lake during the daytime.

LV, Malawi, and Tanganyika in Eastern Africa are affected by local to large-scale circulation. Differential solar irradiance heating over land and water strengths local circulation. [26] showed lake hydrodynamics redistributed surface water temperature according to wind patterns. [27] showed 5-day rainfall accumulation distribution highly sensitive to air temperature variation. Previous studies demonstrated lake surface temperature changes in rainfall patterns. Their coupled atmosphere-lake model yielded more realistic circulation. Their results have also shown an LST pattern with an eastward temperature gradient opposite to the lake bathymetry with lower lake depth westward and higher ones eastward. Simulations of rainfall patterns with LST yielded better results than observed ones.

[28] studied the temporal variability of rainfall in the LV watershed and obtained long-term monthly rainfall averages in LV between 1903 and 2006. The number of weather stations increased from 1903 to 1975. Unfortunately, the number of weather stations has decreased since 1976. The west side of the lake shows higher rainfall accumulation with a maximum in April, November, and December. Rainfall accumulation decreases away from LV. Drier conditions dominate at the south side of LV between June and August while the northeast side precipitation is maximum between April and August. Monthly precipitation accumulation is highest in April all around LV. Other studies have shown maximum rainfall accumulation between March and May and October and December with rainfall patterns similar to CMORPH (**Figure 2**). [29] showed CMORPH rainfall spatial-temporal distribution pattern over Nile Watershed was fairly good but tended to overestimate precipitation under complex topography, though with better performance over the equatorial region (~3˚S to 1˚N). CMORPH overestimation precipitation up to 200 $mm \cdot yr^{-1}$ in Rift Valley in central LV and underestimation it between 50 $mm \cdot yr^{-1}$ and 250 $mm \cdot yr^{-1}$ east and south of mountains west of LV as in [29]. A CMORPH precipitation climatology with complete datasets from 2000 to 2014 is present in this study for LV watershed and surroundings (**Figure 1(a)**).

2. Methodology

CMORPH and LIS datasets between 2000 and 2014 are used to obtain a precipi-

tation climatology within the larger domain and Hovmöller diagrams within a smaller subdomain centered in LV in Equatorial Africa (Figure 1(a)). A brief description of the datasets is presented below.

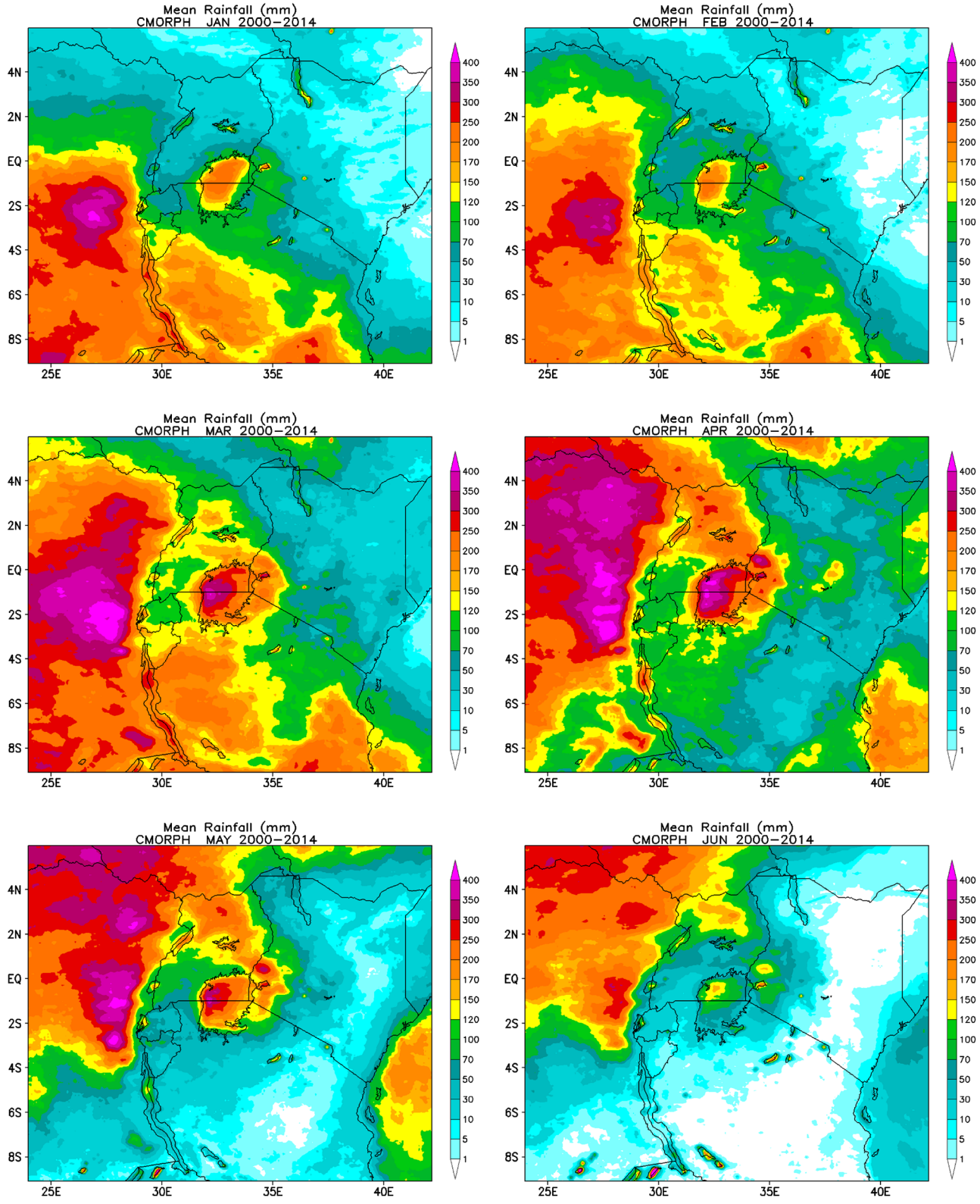

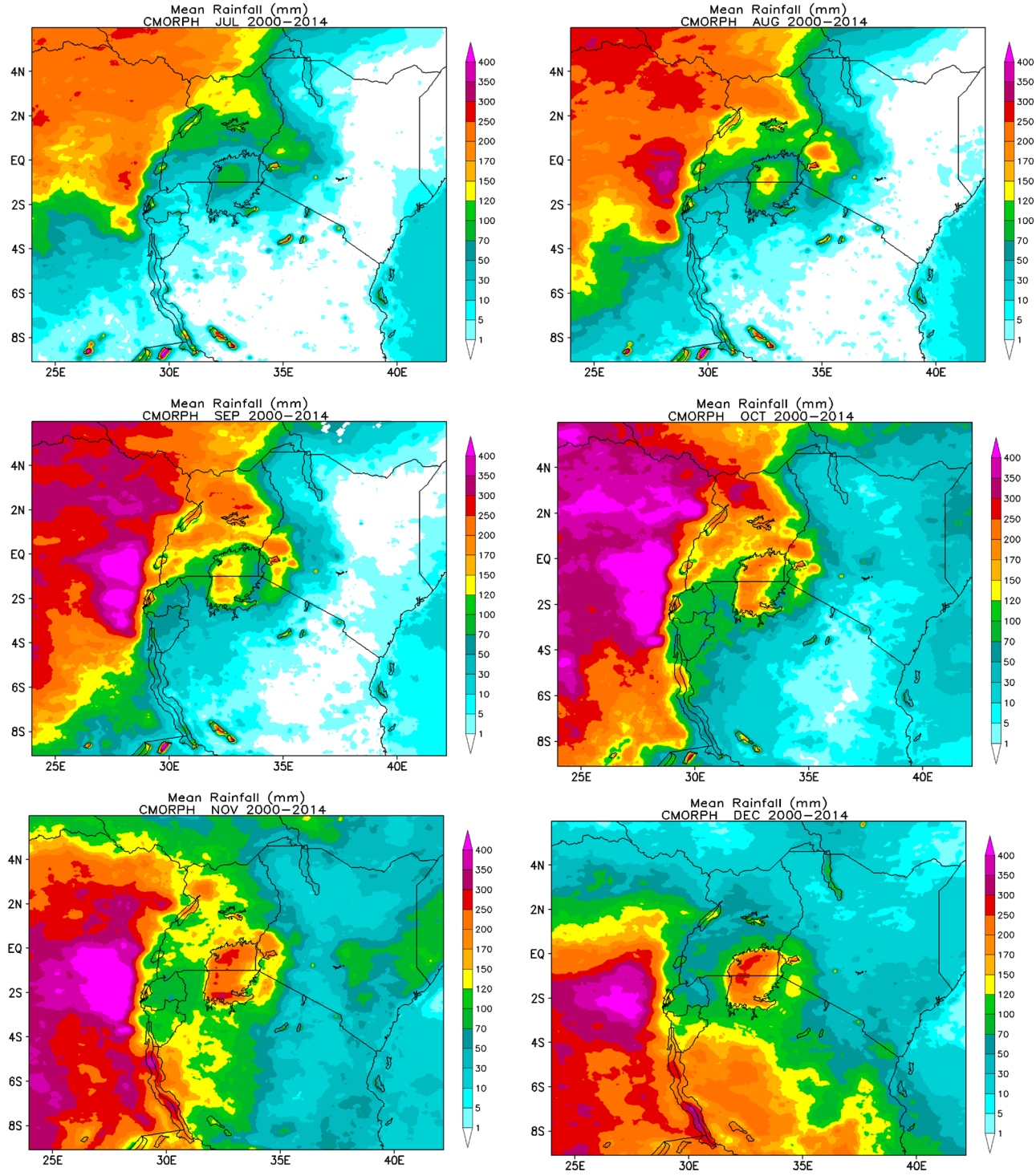

Figure 2. Monthly CMORPH precipitation average field (mm) from January 2000 to December 2014. Latitudes, longitudes, geography boundaries are shown. Color scales are indicated.

2.1. The CMORPH Technique

CMORPH provides high spatial (~8 km) and temporal (30 min.) rainfall estimation globally from 60˚S to 60˚N. This method combines passive microwave (PMW) rainfall rate estimation with IR advection described by [1]. The mean

difference between CMORPH and other satellite-based rainfall estimation methods (e.g., TRMM) is the use of an IR estimated wind vector for advecting rainfall rates. **Figure 1(b)** shows the study area with CMORPH yearly rainfall average in Equatorial Africa between 2000 and 2014. Hourly, daily, monthly, and yearly precipitation accumulation was obtained to analyze precipitation regimes and frequencies for different precipitation accumulation thresholds.

2.2. Hovmöller Diagrams

The coherence, longevity, and length analysis of convective systems over Equatorial Africa and Lake Victoria from time-longitude diagrams of hourly-CMORPH rainfall estimation are similar to the ones for Amazon Basin described in [3]. That is, 2D autocorrelation functions rectangular in one direction and cosine-weighted in the perpendicular direction are fitted to the rainfall data in Hovmöller space. It is stepped through all 1-hour per 0.2˚ all positions. So, contiguous fits define the coherent span, duration, and propagation characteristics for each rain streak [3].

A rainfall and correlation minimum thresholds are required to the fit to become part of the statistics. The analysis area was selected considering the genesis of most convective systems triggered east of Lake Victoria. An autocorrelation function was fitted to each rainfall streak in the Hovmöller diagram to obtain its span, duration, and phase speed. The autocorrelation function is rectangular along with a given rain streak and cosine-weighted perpendicular to it. This function is stepped through all time-longitude positions at 0.16˚ and 30-min. steps to obtain contiguous rain streak with autocorrelation > 0.35 as in [30] [4] [31]. Hourly time-longitude streaks slanted eastward and westward indicates propagating convective systems. In general, stationary ones start in the daytime around Lake Victoria between evening and early morning. The latter yields stronger winds and higher precipitation over the LV and surroundings. Episodes of organized convection with mean hourly precipitation rate > 0.1 $mm \cdot h^{-1}$ were considered to compute spans, duration, and phase speeds. Convective systems starting between 24˚E and 27˚E were not included in the analysis just the ones longer than 300 km. Episodes starting before 27˚E and ending after 24˚E were considered in the statistics.

2.3. Lightning Imaging Sensor (LIS)

The diurnal cycle of lightning and the total number of flashes per pentad from 1998 to 2013 were obtained from LIS climatology datasets at 0.1˚ spatial resolution available for Equatorial Africa. The time of maximum rainfall and lightning activity are in phase and are highly correlated according to [32]. The LIS has also been used to evaluate other lighting networks such as the WWLLN [33].

3. Results and Discussion

The precipitation climatology and precipitation frequencies for arbitrary thre-

sholds are analyzed in this Section. A total of 33,189 episodes of organized convective were obtained from Hovmöller diagrams between 2000 and 2014 to compute their spans, durations, and phase speeds.

3.1. CMORPH Rainfall Climatology

The yearly precipitation average in Fig 1b indicates higher precipitation accumulation (>4000 mm·yr^{-1}) in Congo Forest and lower (< 200 mm·yr^{-1}) accumulation eastward from the Rift Valley and mountains (**Figure 1(b)**). Secondary maxima are located over LV (3000 mm·yr^{-1}) and other lakes: Tanganyika (6.3˚S, 29.6˚E), Rukwa (7.9˚S, 32.3˚E), Mweru (8.9˚S, 28.8˚E), Kivu (2.0˚S, 29.2˚E), Edward (0.3˚S, 29.6˚E), Albert (1.7˚N, 30.9˚E), Kwanja (1.8˚N, 32.8˚E), Kyoga (1.5˚N, 32.9˚E), and Kojweri (1.6˚N, 33.2˚E). Higher precipitation over lakes in the region is caused by differential heating and local circulation as in [34] and [26]. A few instances of these heavy rainfall episodes over LV are shown in Section 3.2 where the Easterlies tend to displace the precipitation maximum westward.

Monthly precipitation average fields are shown in **Figure 2** for Equatorial Africa. The region can be divided into north and south regions by the 0˚ latitude passing just north of LV and into west and east regions by the 33˚E longitude passing in the middle of LV. There is a sharp contrast between monthly precipitation between the east region (very dry) and wet (very wet) especially between June and September and between September and November, respectively. The annual north-south march of the Intertropical Convergence Zone (ITCZ) is also apparent. Maximum monthly precipitation occurs in April, May, and October further north November, December, and January further south, and in It is further north in April and further south in December. Monthly precipitation over LV is higher in March, April (maximum), and May, and lower in June, July (minimum). Thus, precipitation accumulation is related to the LV annual cycle of solar diabatic heating of the Equatorial region in the Southern Hemisphere. According to [35], the main mode of moisture transport is by the mean zonal flow estimated in −11 m·s^{-1}·kg^{-1} while transients are null in the region. The vertically integrated divergence of water or the atmospheric branch of the hydrological cycle varies from about −1000 mm·yr^{-1} on the east side and 1000 m·yr^{-1} in the east between December and January while between June and August it is about 2000 m·yr^{-1} in the entire region. This moisture divergence is in conjunction with a prevailing southeast flow of moisture from continental Africa. Less low precipitation accumulation at the east of LV between March and May and between October and December is associated with the prevailing northeast flow of moisture from the Indian Ocean. Precipitation is higher over the ocean close to shore between March and April. Thus, the monthly spatial-temporal precipitation patterns in the analysis area are consistent with the general circulation and thermodynamics modified by local circulation induced by differential heating close to lakes, especially in LV and its surroundings as is analyzed in the next Sections.

3.2. CMORPH Hourly Rainfall Frequency

Frequencies of CMORPH hourly precipitation accumulation thresholds of 1.0 mm, 2.0 mm, 5.0 mm, 10.0 mm, and 20.0 mm were obtained between 2000 and 2014. Figure 3 shows hourly spatial frequencies of hourly precipitation accumulation > 1.0 mm in April when the precipitation is maximum, over LV (Figure 2).

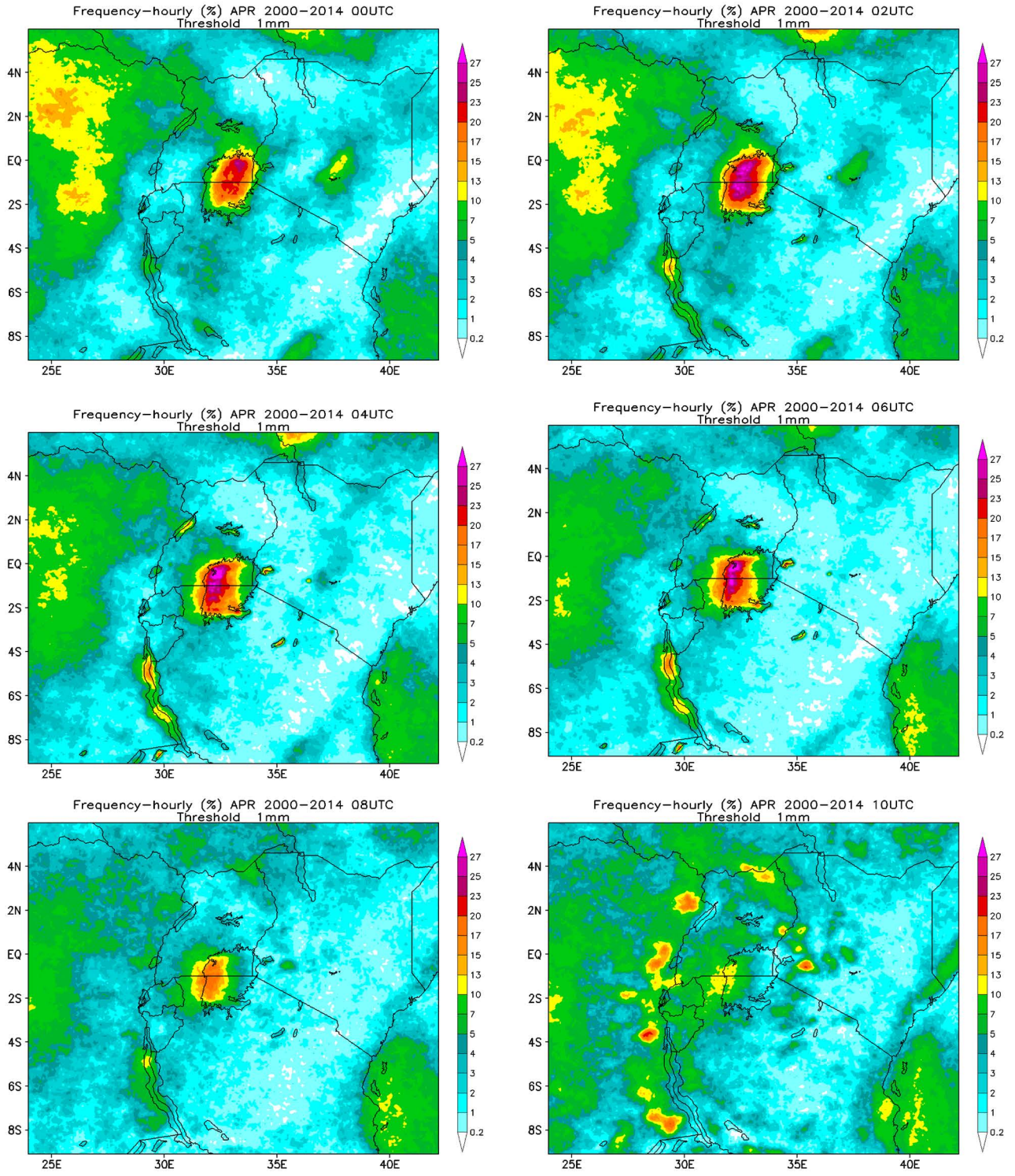

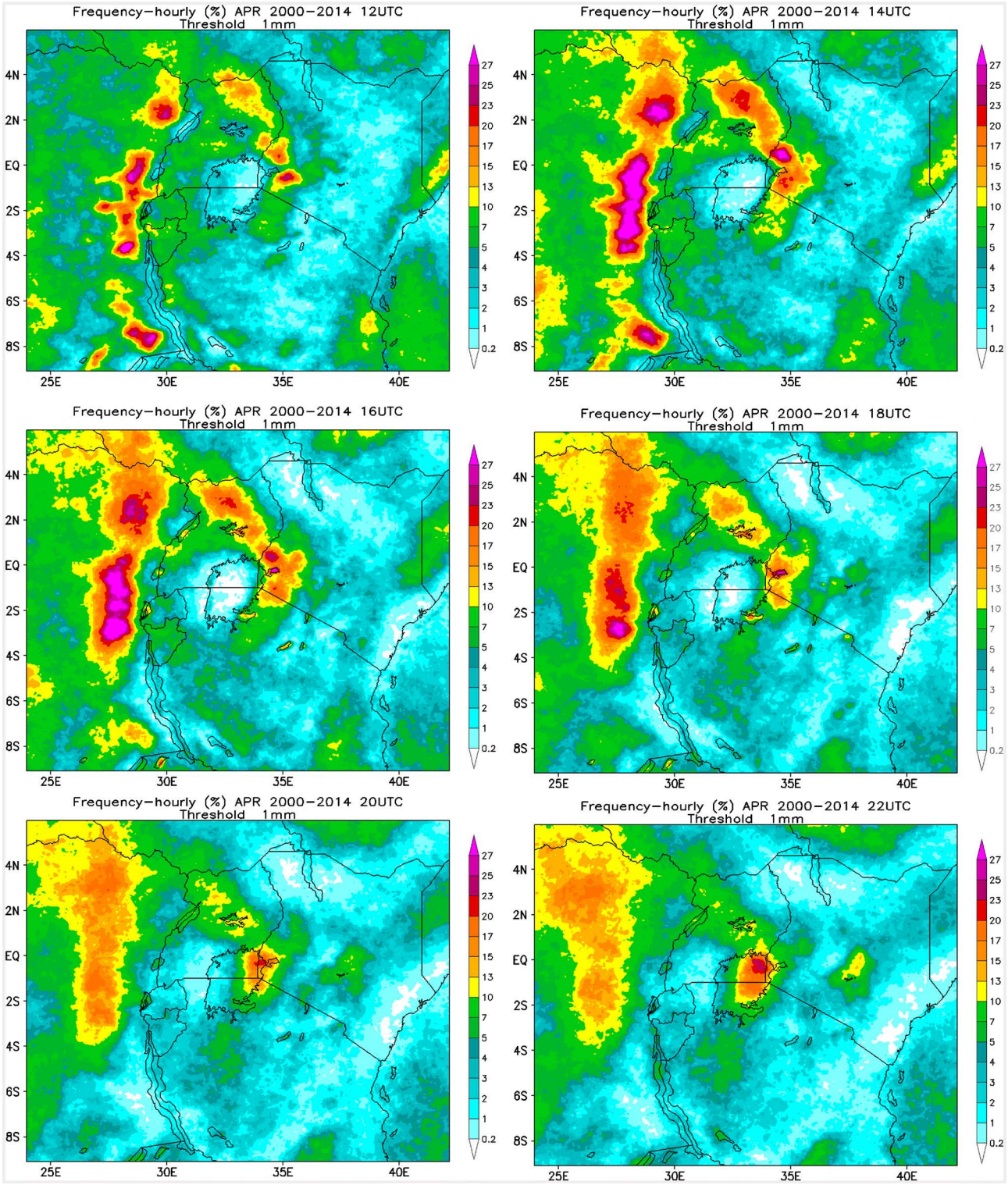

Figure 3. Hourly frequency average (%) of CMORPH hourly rainfall rate > 1 mm·hr^{-1} for April between 2000 and 2014. Latitudes, longitudes, geography boundaries, time (×100 UTC), and color scale are shown.

A persistent maximum frequency over Lake Victoria can be seen from 2200 UTC to 0800 UTC the next day. Similar hourly precipitation frequency patterns are observed for other precipitation thresholds and months but a band of higher

frequencies following the ITCZ. Convection west of the Rift Valley occurs between mid-afternoon and evening, while over the lakes is triggered between evening and early morning (Figure 3).

Other surrounding lakes have high hourly precipitation accumulation frequencies between 0400 UTC and 0600 UTC. While the frequency of hourly precipitation accumulation over Lake Victoria is a minimum between 1200 UTC (1500 LT) and 1800 UTC (2100 LT), it is maximum at its east and over Congo Forest. Hourly frequency of hourly precipitation accumulation increases over the mountains ~35˚E between 1200 UTC and 1800 UTC associated with valley-mountain circulation [27]. As convection progresses westward in the night hours, it decays downwind over Lake Victoria, but it intensifies again induced by lake-land breeze circulation.

The maximum convective activity over Lake Victoria occurs westward late in the evening and early morning and dissipates before reaching its west border. An almost stationary north-south line of higher hourly precipitation frequency is over Congo Forest between 1200 UTC and 2200 UTC associated with the diurnal cycle of convection. Figure 4 shows frequencies of hourly precipitation accumulation > 20 mm at 0300 UTC in April and 0400 UTC in November when frequencies are maxima over LV, respectively. Most intense episodes of convection occur in the southwest border of LV in March, May, October, and November (not shown). Figure 5 shows an instance of westward propagating episodes of convection. The Hovmöller diagram indicates six more intense episodes of convection starting over Lake Victoria between 28 April and 7 May 2010. As will be seen, their underlying thermodynamics can be inferred from spatial-temporal characteristics.

3.3. Organized Convection Features

Long-lasting westward propagating streaks of organized convection move across

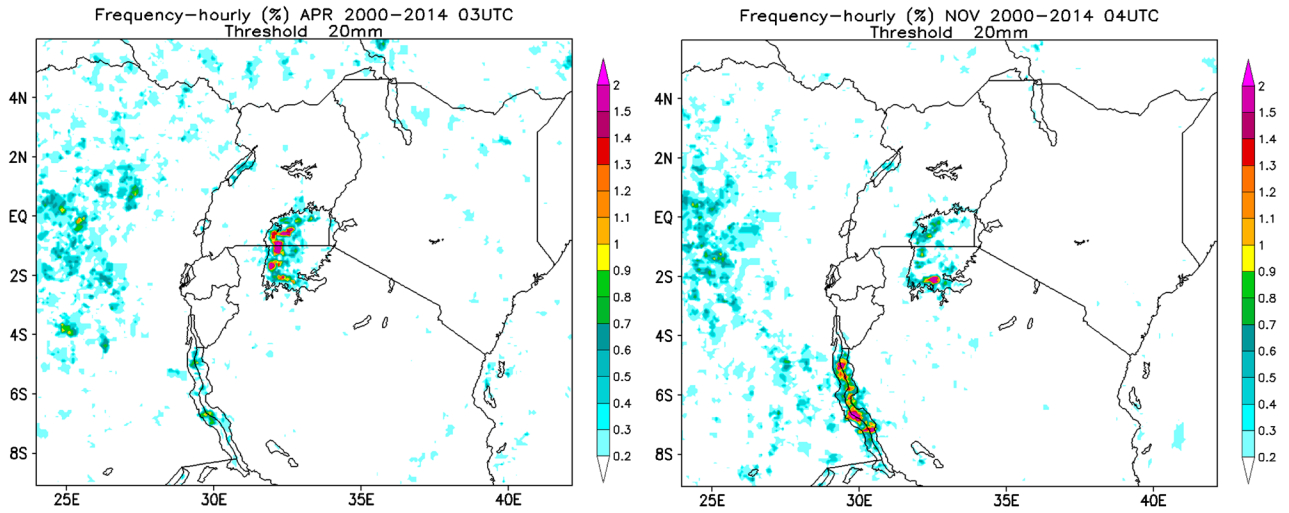

Figure 4. Similar to Figure 3 but for CMORPH hourly rainfall rate > 20 mm hr-1 for 0300 UTC on April (left) and 0400 UTC in November (right).

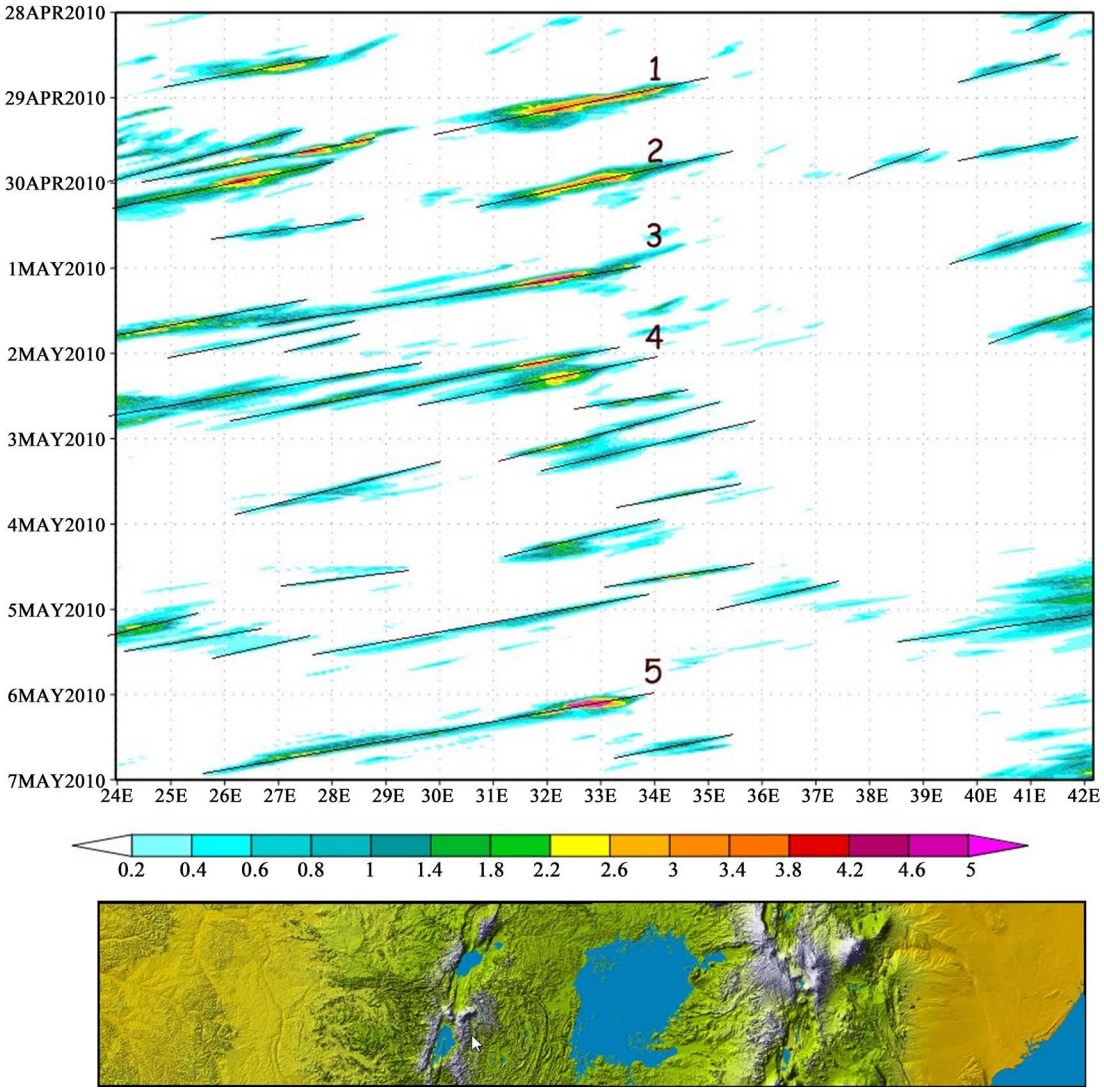

Figure 5. Hovmöller time-longitude diagram of hourly GMOPRH precipitation averaged between latitudes 3˚S and 1˚N (**Figure 1(a)**) from 0000 UTC on 28 April to 0000 UTC on 07 May 2010. Longitudes, dates, and color scale are indicated. Numbers indicate the sequence of organized convection starting over Lake Victoria. The corresponding topographic map (**Figure 1(a)**) is shown below the diagram. Bodies of water in blue, mountains in greyscale.

Equatorial Africa and over LV within the rectangle of **Figure 1(a)**. These systems tend to last more than 50 hr. in March, April, October, and November as indicated by Hovmöller diagram analysis. Short-lived intense convective systems are located over southwest Lake Victoria between 0300 UTC and 0600 UTC in March, April, October, and November (**Figure 4** and **Figure 5**). Widespread convection over Congo Forest is maximum in early to midafternoon as induced by the diurnal cycle of solar diabatic heating.

Figure 6 shows the time-longitude diagram for a one-hour rainfall accumulation average in a 48-hr period computed with CMORPH rainfall estimation in the Equatorial Africa domain (**Figure 1**) between latitudes 3˚S to 1˚N from 2000 to 2014. It indicates the diurnal cycle of convection. Widespread deep convec-

tion across Equatorial Africa starts over mountain ranges triggered by differential heating late in the afternoon and evening. As it propagates westward, land breeze convergence and evaporation over LV re-intensifies convection over the western edge of Rift Valley as it propagates towards Congo Forest at faster phase speed though and so lower precipitation accumulation between 32˚E and 29˚E during the morning before diabatic heating increases. Differential heating over mountains triggers deep convection rapidly at the west edge of the Rift Valley in the early afternoon, a plausible explanation for high precipitation accumulation in Congo Forest.

Organized convection can be affected by equatorial waves as described by [36] and [37]. Local diabatic heating and evapotranspiration are thermodynamically reinforced by Equatorial Africa waves such as internal gravity waves, Kelvin, and Rossby waves as in [38]. The Indian Ocean is the main water vapor source to the western Rift Valley as well as LV evaporation and rainforest evapotranspiration. These variable spatial-temporal mechanisms are secondary to the diurnal cycle of diabatic heating over Lake Victoria. In general, equatorial waves phased locked with organized convection and boundary layer easterlies fluxes. Topographic features tend to amplify (mountains) and to reduce (valleys) precipitation. Furthermore, Kelvin waves might augment easterly moisture advection since its propagation is preceded by easterly low-level anomalies followed by low-level westerly anomalies by increasing convergence and so triggering thunderstorms in the Congo basin according to [39].

Organized convection varies in duration, phase speed, and span. Some are intermittent with variable phase speed and span. Intermittent precipitating patterns propagate eastward transversally to westward prevailing moving systems similar to a Kelvin wave moving by the region, constructively interacting with the diurnal cycle over Equatorial Africa, including LV night convection. They are much less frequent than Rossby waves [15]. [40] and [41] indicate Kelvin equatorial waves propagate eastward rapidly by creating easterly trade winds associated with direct thermal circulation (Walker type) with updrafts over heat sources and downdrafts eastward.

The diurnal cycle becomes less of a defined pattern during the propagation of Kelvin wave trains. They tend to dry the environment around weather systems. Seemingly chaotic precipitation patterns in Equatorial Africa become more organized by equatorial wave effects and easterlies thermodynamic forcing. There are also fewer westerly waves propagating through Equatorial Africa. Some westward barotropic waves are intense and long-lived as indicated by precipitation streaks in **Figure 5**. For instance, the one starting at 34.5˚E on 30 April 2010 propagates over 1000 km to Rift Valley and Congo Forest. Convection intensifies during the diurnal cycle in Equatorial Africa. This wave pattern can be associated with a 5-day Rossby-Haurwitz wave [42].

The mountain range east of LV tends to intensify moving Rossby waves. Westward waves such as Kelvin and Madden-Julian oscillation (MJO) can excite

Rossby waves by reducing stability and increasing lower troposphere convergence [43]. Figure 6 time-longitude diagram of one-hour CMORPH precipitation accumulation estimation averaged in a 48-hr period in the Equatorial Africa domain shown in Figure 1 between latitudes 3˚S to 1˚N from 2000 to 2014. Maximum precipitation is west of Rift Valley. A second maximum is in East LV at 3˚S and 1˚N, where easterlies waves pass through. Convection is weak between LV and Congo Forest. However, it intensifies just west of Rift Valley in association with the diurnal cycle of diabatic differential heating.

Lakes as small as 10-km in diameter alter the rainfall distribution around them [19]. Precipitation is maximum east of LV and over mountains ~34.5˚E and LV ~32˚E. A high precipitation pattern in the west of Rift Valley is caused by the diurnal cycle through with phase shift. High precipitation is over LV at nighttime and early morning. There are two other high precipitation cores associated with 850-hPa easterly waves in the late afternoon. Indeed, the average 850-hPa wind field shows a broader band of easterlies in the latitudinal domain all year long with variable intensity (not shown).

The precipitation maximum west of Rift Valley in Figure 6 coincides with downstream the watershed, upstream the mean 850-hPa wind field. There are secondary precipitation peaks over LV, 12-hr ahead of the one at the west of Rift Valley, and over the mountain range east of LV. Minima precipitation occurs in the morning and afternoon hours west of Rift Valley and LV, respectively. The seasonal variation of the diurnal cycle is remarkable with significant differences in amplitude, but almost no difference in phase (not shown).

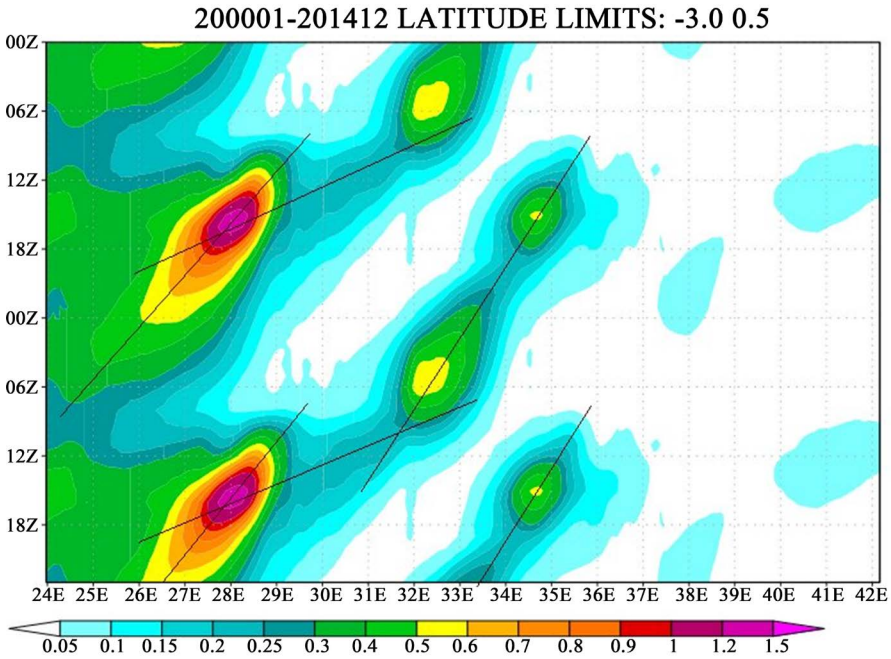

Figure 6. Hovmöller time-longitude diagram for one-hour rainfall accumulation average in a 24-hr period computed with CMORPH rainfall estimation in Equatorial Africa domain (Figure 1) between latitudes 3˚S to 1˚N from 2000 to 2014. Longitudes, hour (×100 UTC), and color scale are indicated.

The frequency of hourly rainfall greater than 1 mm is highest with 50% (30%) frequency in fall and spring west of Rift Valley (LV) and minimum in June with about 20% (12%) frequency west of Rift Valley (LV). Extremely dry conditions with low precipitation frequency year around east of 36˚E. Figure 4 shows an example of the diurnal cycle of frequencies of hourly rainfall greater than 1 mm between 0000 UTC on 28 April and 0000 UTC on 07 May 2010. Other months have similar patterns (not shown). Figure 7 shows the diurnal cycle of LIS lightning strikes highly correlated with the CMORPH rainfall climatology. The maximum number of flashes is between 0500 UTC and 0800 UTC over LV just east of the maximum in precipitation. This small spatial lag might be caused by LIS smoothing method. The instances shown in this section illustrate the main features of organized convection over Equatorial Africa. A complete statistic of all propagating convective systems from 2000 to 2014 is shown in the section below.

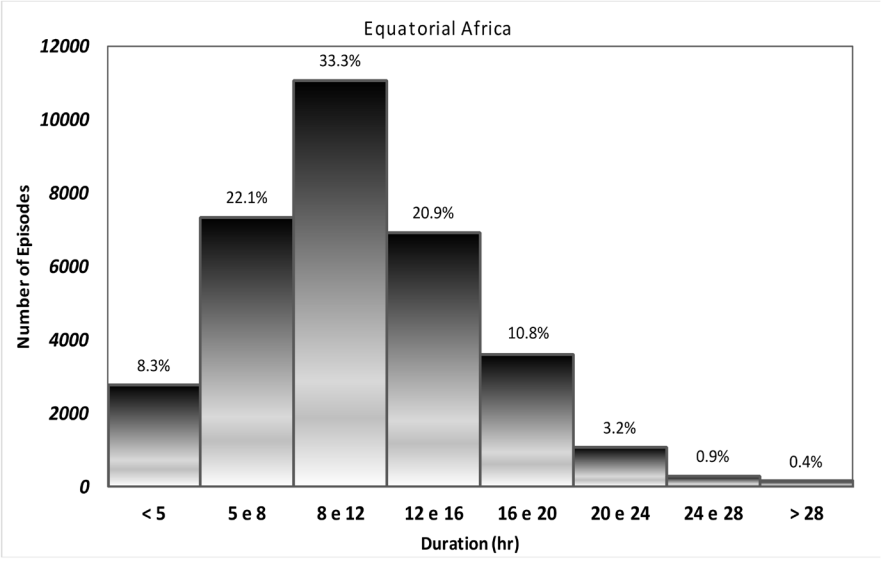

(a)

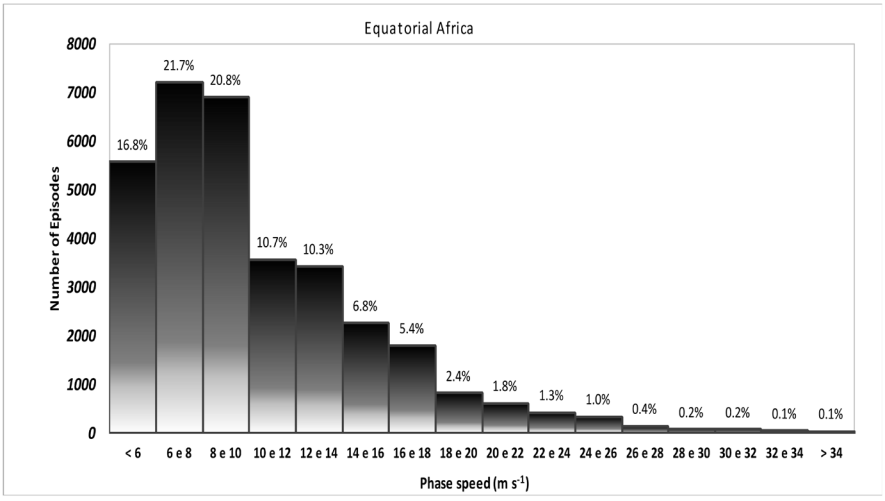

(b)

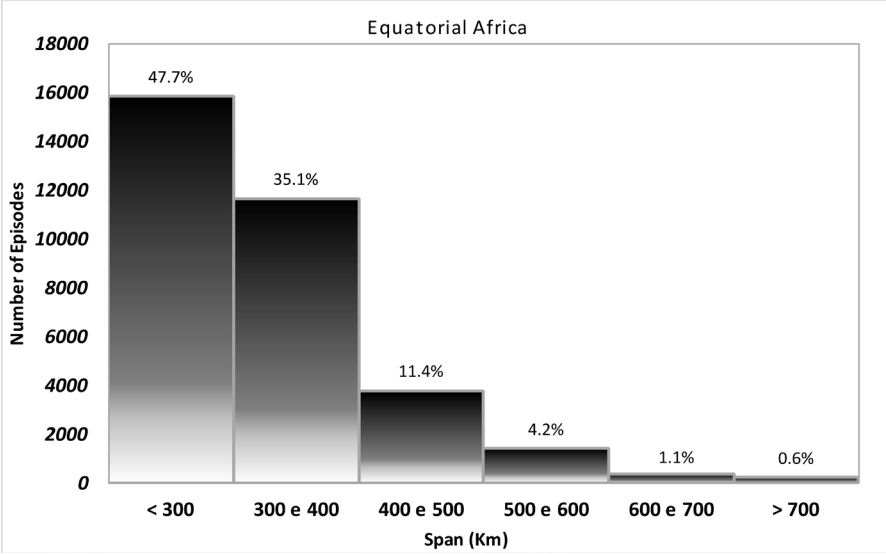

(c)

Figure 7. Frequency distribution of duration (top), phase speed (middle), and span (bottom) of westward episodes of organized convection in Equatorial Africa (**Figure 1**) between December 2000 and 2014. A total of 33,189 episodes were computed. IU indicated in abscissas.

3.4. Span, Phase Speed, and Duration Statistics

Figure 8 shows the frequency distribution of duration, phase speed, and span of all westward propagating episodes of organized convection between 2000 and 2014. Frequencies are higher between March and May and between October and November and lower in July and August linked to ITCZ. Since there are 5 - 10 eastward propagating episodes a year number, they were included in the present study. The average span, phase speed, and duration of westward episodes are 332 km, 10.3 $m{\cdot}s^{-1}$, and 10.7 hr, respectively. The frequencies of phase speeds < 6 $m{\cdot}s^{-1}$, between 6 $m{\cdot}s^{-1}$ to 10 $m{\cdot}s^{-1}$ and > 30 $m{\cdot}s^{-1}$ are 17%, 40% and 0.5%, respectively, while of spans < 300 km and > 500 km are 50 % and 6%, respectively, and durations between 8 hr to 16 hr, > 20 hr and < 5 hr are 50%, 5% and 8%, respectively.

There were 3515 episodes with spans > 600 km (**Figure 8(d)**) caused by the merging of smaller span episodes with a correlation > 0.35. These longer-span episodes are caused by longer equatorial waves triggering short-lived convective rainfall that dissipates and intensifies, later on, depending on the location to where they move. These longer span episodes have average phase speed and duration of 12.1 $m{\cdot}s^{-1}$ and 19 hr, respectively. They have lower phase speeds than the ones under synoptic-scale forcing and start in between LV and Congo Forest in association with local circulation and the diurnal heating cycle.

Spans < 500 km tend to propagate faster, though the contrary depends on underlying dynamic and thermodynamic conditions. The mean phase speed of episodes with spans > 600 km is higher than those < 500 km in the span. The frequency spectrum of phase speeds is broader (narrower) for longer (shorter) durations and spans, but there are some episodes with higher phase speeds and

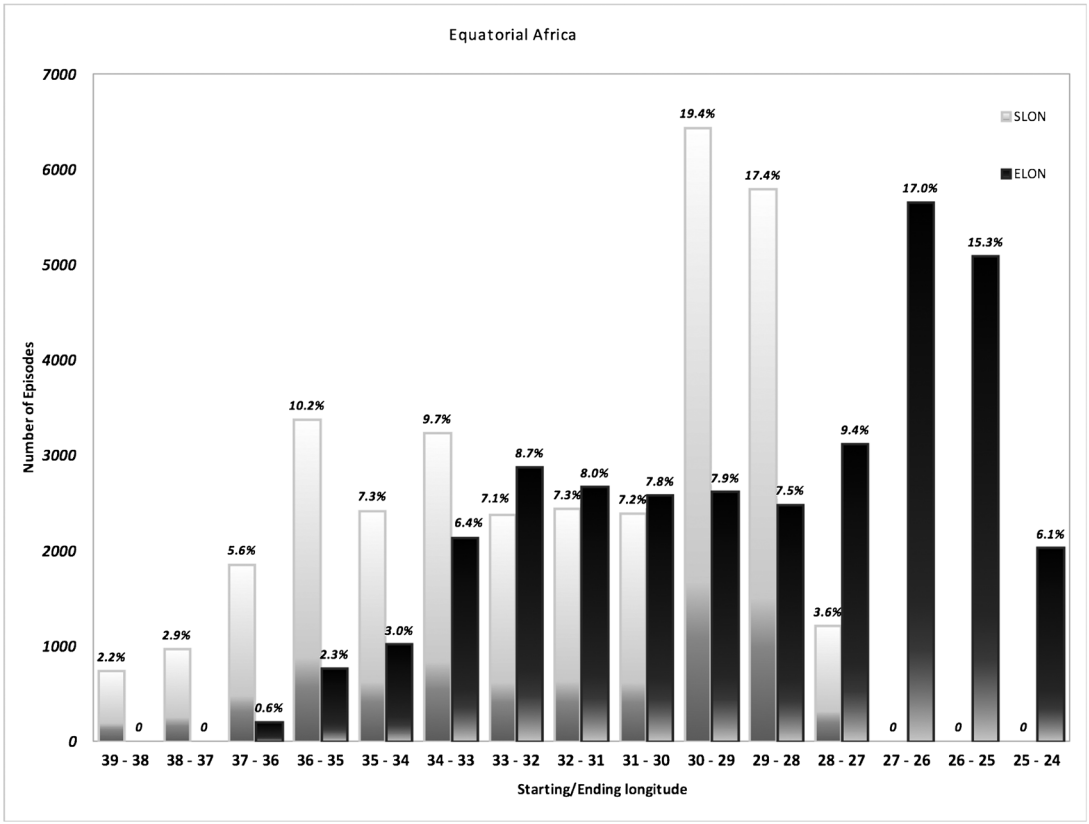
Equatorial Africa
Number of Episodes
Starting/Ending longitude
SLON
ELON
39 - 38
38 - 37
37 - 36
36 - 35
35 - 34
34 - 33
33 - 32
32 - 31
31 - 30
30 - 29
29 - 28
28 - 27
27 - 26
26 - 25
25 - 24

(a)

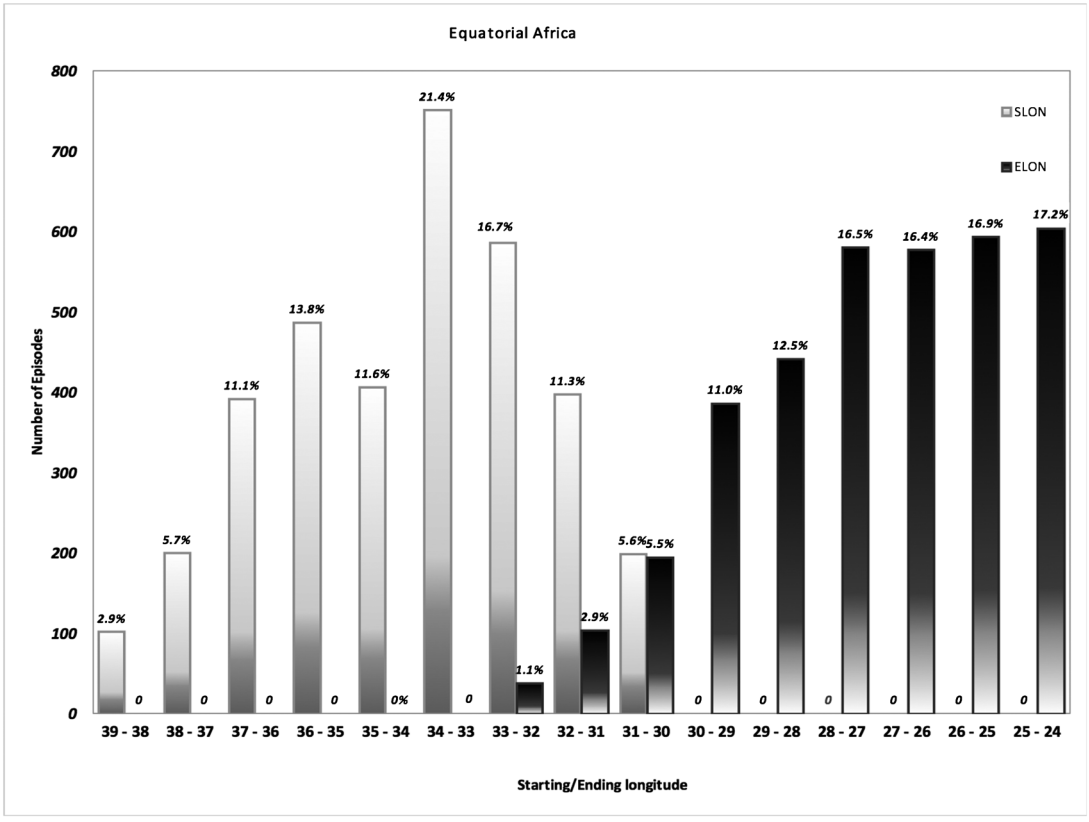
Equatorial Africa
Number of Episodes
Starting/Ending longitude
SLON
ELON
39 - 38
38 - 37
37 - 36
36 - 35
35 - 34
34 - 33
33 - 32
32 - 31
31 - 30
30 - 29
29 - 28
28 - 27
27 - 26
26 - 25
25 - 24

(b)

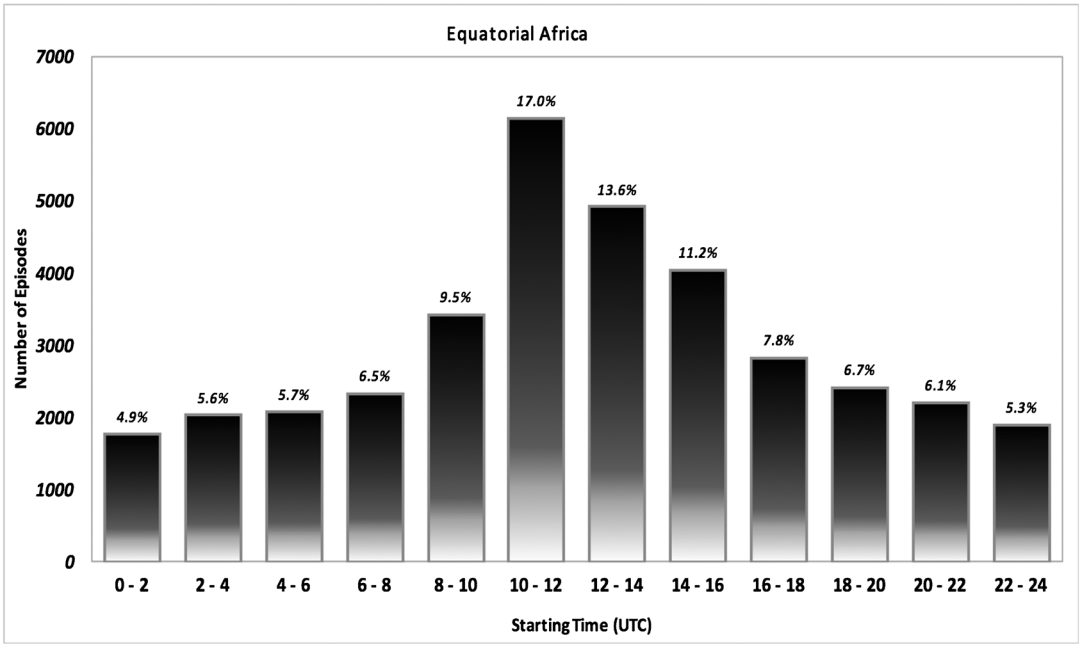

(c)

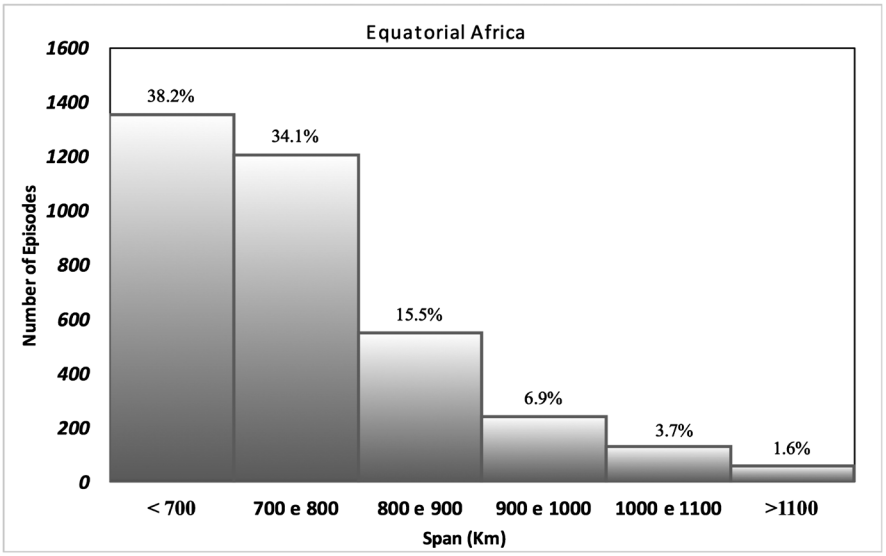

(d)

Figure 8. Frequency distribution of starting and ending longitudes (deg.) of organized convection in Equatorial Africa (**Figure 1**) for all spans (a) and spans > 600 km (b) between latitudes 0.5˚S to 3.0˚N, starting times (c) and frequency of spans (d).

long spans and durations.

Westward propagating episodes in Equatorial Africa starting in the late afternoon in east LV strengths early morning over LV and trigger convection west of Lake Kivu during the afternoon. Over LV and west of the Rift Valley, the episodes tend to increase phase speeds given less friction force over LV's large water surface and almost flat terrains west of Lake Kivu.

LV evaporation advected westward increases rainfall over Congo Forest dur-

ing the afternoon (not shown) due to convectively coupled equatorial waves [41]. Easterlies barotropic energy advection coupled with the diurnal cycle might yield deep convection over Congo Forest [44]. The maximum precipitation over Congo Forest is at the same latitude band of LV. Less precipitation is outside of this latitude band by almost half the one over Congo Forest.

Therefore, LV evaporation intensifies convection associated with passing equatorial waves, increasing precipitation accumulation by 70% west of it. Many short-span episodes start west of LV strength over it and dissipate east of LV. The cold pool of thunderstorms reaches the western edge of Rift valley early to middle afternoon and triggers new ones. These episodes are separate in the Hovmöller diagram because they dissipate between LV and western of Rift Valley, although one is related to the other.

About 50% and 30% of the convective episodes with spans > 600 km (about the distance between middle LV to Congo Forest) start over LV and east of LV, respectively, and trigger convection also in Congo Forest. It can be inferred from **Figure 8** the association between rainfall over LV and Congo Forest through equatorial Rossby waves. About 30% of the convective episodes initiating east of LV yield rainfall over it. Episodes initiated over LV (24%) induced rainfall west of Lake Kivu by passing waves (**Figure 9**). It is an area of low precipitation between LV (32˚E) and East of Congo Forest (29˚E) as seen in **Figure 1(a)**. Another evidence that episodes triggered over LV generally have a greater impact over Congo Forest during the afternoon is the associated phase speed and timing, enough for them to reach Congo Forest during the afternoon.

Additionally, when considering spans > 600 km, the correlation between a Hovmöller streak passing over LV and east of Congo Forest is greater than 0.35. All episodes beginning in the afternoon east of LV (30%) intensifies mountain breezes east of LV. Later, they trigger thunderstorms over it at dawn. About 30% of the episodes were triggered between late evening and dawn over LV or just east of it (**Figure 8(a)**). Local circulation triggers 30% of westward episodes and might trigger thunderstorms over Congo Forest. This interesting result shows how large lakes such as LV can influence rainfall patterns hundreds of kilometers away. Some studies have shown lakes larger than 100 km yield lake breezes similar to sea breezes propagating hundreds of kilometers away from them.

4. Conclusions

New hourly high spatial-temporal resolution satellite-derived precipitation datasets by CMORPH between 2000 and 2014 were used in this present work to study organized convection in Equatorial Africa with emphasis on Lake Victoria, a very important body of water in Africa. The results indicate the impact of the LV in climate hundreds of kilometers away in the Congo Forest. Hovmöller analysis indicates three main triggering areas of organized convection: 1) over mountain ranges east of LV, triggered by differential heating during afternoon as observed in the CMORPH rainfall field and the LIS lightning flash density field;

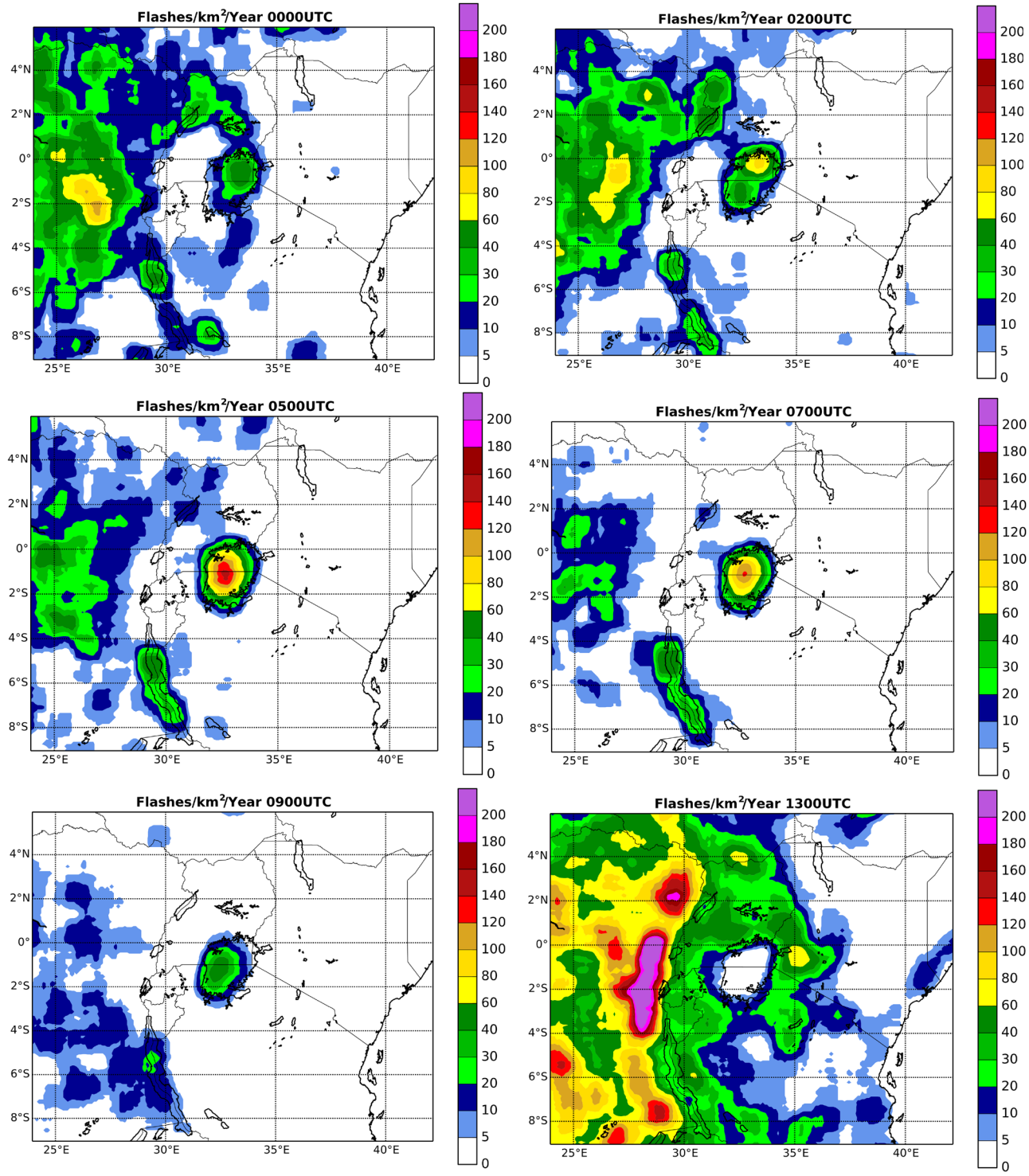

Figure 9. Hourly lightning density of flashes ($km^{-2} \cdot yr^{-1}$) average field in Equatorial Africa. Longitudes, latitudes, geographic boundaries, time, and color scale are shown. Source: NASA, http://lightning.nsstc.nasa.gov/data/data_lis-vhr-climatology.html.

2) west of LV, triggered by the interaction between local circulation, mountain breeze and land breeze induced during dawn and; 3) west of western Rift Valley. Episodes of organized convection triggered by equatorial waves passing by LV are longer than 600 km in the span. They strengthen over LV and impact thun-

derstorms to Congo Forest with the highest incidence of lightning. Hovmöller time-longitude diagrams were used to compute starting and ending longitudes, span, phase speeds, and duration of organized convection, a total of 33,189 rain streaks in Equatorial Africa in 15 years. Westward propagating episodes are dominant features with the average span, phase speed, and duration of 332 km, 10.3 $m \cdot s^{-1}$, and 10.7 hr., respectively. Episodes with spans > 600 km have average phase speed and duration of 12.1 $m \cdot s^{-1}$ and 19 hr, respectively.

These long-lived transient systems in Equatorial Africa are triggered by east-west differential diabatic heating where systems such as cold fronts and cyclones are absent. Phase speeds tend to increase east of LV and decrease west of LV to Congo Forest. The results suggest LV impacts Congo Forest given its large water surface. Convergence in west LV tends to decrease phase speeds. Further work on high-resolution mesoscale numerical simulation of local circulation and very deep convection in LV will be published elsewhere.

Acknowledgements

The authors are grateful to CPC/NCEP for providing high-resolution CMORPH datasets and GHRC for providing climatological LIS datasets. The F.V. was supported by Conselho Nacional de Desenvolvimento Científico e Tecnológico (CNPq) under grants 302349/2014-6 and 162576/2015-3 and by Fundação Coordenação de Aperfeiçoamento de Pessoal de Nível Superior (CAPES). A.J.P.F was sponsored by CNPQ under grant 302349/2017-6.

Conflicts of Interest

The authors declare no conflicts of interest regarding the publication of this paper.

References

[1] Joyce, R.J., Jonawiak, E.J., Arkin, A.P. and Xie, P. (2004) CMORPH: A Method That Produces Global Precipitation Estimates from Passive Microwave and Infrared Data at High Spatial and Temporal Resolution. *Journal of Hydrometeorology*, **5**, 487-503. https://doi.org/10.1175/1525-7541(2004)005<0487:CAMTPG>2.0.CO;2

[2] Pereira Filho, A.J., Vemado, F., Vemado, G., *et al.* (2018) A Step towards Integrating CMORPH Precipitation Estimation with Rain Gauge Measurements. *Advances in Meteorology*, **2018**, Article ID: 2095304. https://doi.org/10.1155/2018/2095304

[3] Pereira Filho, A.J., Carbone, R.E., Tuttle, J.D. and Karam, H.A. (2015) Convective Rainfall in Amazonia and Adjacent Tropics. *Atmospheric and Climate Sciences*, **5**, 137-161. https://doi.org/10.4236/acs.2015.52011

[4] Pereira Filho, A.J., Carbone, R. and Tuttle, J. (2014) Convective Rainfall Systems in the La Plata Basin. *Atmospheric and Climate Sciences*, **4**, 757-778. https://doi.org/10.4236/acs.2014.44068

[5] Pereira Filho, A. J., Carbone, R.E., Janowiak, J.E., Arkin, P., Joyce, R., Hallak, R. and Ramos, C.G.M. (2009) Satellite Rainfall Estimates over South America—Possible Applicability to the Water Management of Large Watersheds. *Journal of the American Water Resources Association* (*JAWRA*), **46**, 344-360. https://doi.org/10.1111/j.1752-1688.2009.00406.x

[6] Janowiak, J.E., Kousky, V.E. and Joyce, R.J. (2005) Diurnal Cycle of Precipitation Determined from the CMORPH High Spatial and Temporal Resolution Global Precipitation Analyses. *Journal of Geophysical Research*, **110**, D23105. https://doi.org/10.1029/2005JD006156

[7] Kousky, V.E., Janowiak, J.E. and Joyce, R.J. (2006) The Diurnal Cycle of Precipitation over South America Based on CMORPH. *Proceedings of* 8 *ICSHMO*, *INPE*, Foz do Iguaçu, 1113-1116.

[8] Spigel, R.H. and Coulter, G.W. (1996) Comparison of Hydrology and Physical Limnology of the East Africa Great Lakes: Tanganyika, Malawi, Victoria, Kivu and Turkana (Concerning Some North American Great Lakes). In Johnson, T.C. and Odada, E., Eds., *The Limnology*, *Climatology*, *and Paleoclimatology of the East African Lakes*, Gordon and Breach Publishers, Amsterdam, 103-139. https://doi.org/10.1201/9780203748978-6

[9] Howell, P.P., Lock, M. and Cobb, S. (1988) The Jonglei Canal: Impact and Opportunity. Cambridge University Press, Cambridge.

[10] Yin, X. and Nicholson, S.E. (1998) The Water Balance of Lake Victoria. *Hydrology Science Journal*, **43**, 789-811. https://doi.org/10.1080/02626669809492173

[11] Soula, S., Kasereka, J.K., Geogis, J.F. and Barthe, C. (2016) Lightning Climatology in the Congo Basin. *Atmospheric Research*, **178**-**179**, 304-319. https://doi.org/10.1016/j.atmosres.2016.04.006

[12] Chamberlain, J.M., Bain, C.L., Boyd, D.F.A., McCourt, K., Butcher, T. and Palmer, S. (2013) Forecasting Storms over Lake Victoria Using a High-Resolution Model. *Meteorological Applications*, **21**, 419-430. https://doi.org/10.1002/met.1403

[13] William, K., Chamberlain, J., Buontempo, C. and Bain, C. (2014) Regional Climate Model Performance in the Lake Victoria Basin. *Climate Dynamic*, **44**, 1699-1713. https://doi.org/10.1007/s00382-014-2201-x

[14] Sutcliffe, J.V. (1988) The Influence of Lake Victoria: Climate Change and Variation in River Flows. In: Howell, P.P., Lock, M. and Cobb, S., Eds., *The Jonglei Canal*: *Impact and Opportunity*, Cambridge University Press, Cambridge, 87-99.

[15] Mekonnen, A., Thorncroft, C.D., Aiyyer, A.R. and Kiladis, G.N. (2008) Convectively Coupled Kelvin Waves over Tropical Africa during the Boreal Summer: Structure and Variability. *Journal of Climate*, **21**, 6649-6667. https://doi.org/10.1175/2008JCLI2008.1

[16] Mekonnen, A. (2006) The Role of Kelvin Wave Activity on Convection and Rainfall over Tropical Africa. In: 27*th Conference on Hurricane and Tropical Meteorology*, American Meteorological Society, Monterey, 4D.2. http://ams.confex.com/ams/pdfpapers/108508.pdf

[17] Albrecht, R.I., Goodman, S., Buechler, D., Blakeslee, R. and Christian, H. (2016) LIS 0.1 Degree Very High-Resolution Gridded Lightning Diurnal Climatology (VHRAC). Dataset Is Available Online from the NASA Global Hydrology Resource Center DAAC, Huntsville.

[18] Asefi-Najafabady, S., Knupp, K., Mecikalski, J.R. and Welch, R.M. (2012) Radar Observation of Mesoscale Circulations Induced by the Small Lake under Varying Synoptic-Scale Flows. *Journal of Geophysical Research*, **117**, D01106. https://doi.org/10.1029/2011JD016194

[19] Crosman, E.T. and Horel, J.D. (2012) Idealized Large-Eddy Simulations of Sea and Lake Breezes: Sensitivity to Lake Diameter, Heat Flux, and Stability. *Boundary-Layer Meteorology*, **114**, 573-594. https://doi.org/10.1007/s10546-012-9721-x

[20] Porson, A., Steyn, D.G. and Schayes, G. (2007) Formulation of an Index for Sea Breeze in Opposing Winds. *Journal of Climate and Applied Meteorology*, **46**, 1257-1263. https://doi.org/10.1175/JAM2525.1

[21] Daggupaty, S.M. (2000) A Case Study of the Simultaneous Development of Multiple Lake-Breeze Fronts with a Boundary Layer Forecast Model. *Journal of Applied Meteorology*, **40**, 289-311. https://doi.org/10.1175/1520-0450(2001)040<0289:ACSOTS>2.0.CO;2

[22] Laird, N.F., Walsh, J.E. and Kristovich, D.A.R. (2003) Model Simulations Examining the Relationship of Lake-Effect Morphology to Lake Shape, Wind Direction, and Wind Speed. *Monthly Weather Review*, **131**, 2102-2111. https://doi.org/10.1175/1520-0493(2003)131<2102:MSETRO>2.0.CO;2

[23] Laird, N.F., Desrochers, J. and Payer, M. (2009) Climatology of Lake-Effect Precipitation Events over Lake Champlain. *Journal of Applied Meteorology and Climatology*, **48**, 232-250. https://doi.org/10.1175/2008JAMC1923.1

[24] Zumpfe, D.E. and Horel, J.D. (2006) Lake-Breeze Fronts in the Salt Lake Valley. *Journal of Applied Meteorology and Climatology*, **46**, 196-211. https://doi.org/10.1175/JAM2449.1

[25] Stivari, S.M.S., Oliveira, A.P. and Soares, J. (2005) On the Climate Impact of the Local Circulation in the Itaipu Lake Area. *Climatic Change*, **72**, 103-121. https://doi.org/10.1007/s10584-005-5923-2

[26] Anyah, R.O. (2006) Modeling the Variability of the Climate System over Lake Victoria Basin. Ph.D. Dissertation, North Carolina State University, Raleigh.

[27] Sun, X., Xie, L., Semazzi, F.H.M. and Liu, B. (2014) A Numerical Investigation of the Precipitation over Lake Victoria Basin Using a Coupled Atmosphere-Lake Limited Area Model. *Advances in Meteorology*, **2014**, Article ID: 960924. https://doi.org/10.1155/2014/960924

[28] Kizza, M., Rodhe, A., Xu, C.-Y., Ntale, K.H. and Halldin, S. (2009) Temporal Rainfall Variability in the Lake Victoria Basin in East Africa during the Twentieth Century. *Theoretical and Applied Climatology*, **98**, 119-135. https://doi.org/10.1007/s00704-008-0093-6

[29] Habib, E., Elsaadani, M. and Haile, A.T. (2012) Climatology-Focused Evaluation of CMORPH and TMPA Satellite Rainfall Products over the Nile Basin. *Journal of Applied Meteorology*, **51**, 2105-2121. https://doi.org/10.1175/JAMC-D-11-0252.1

[30] Carbone, R.E., Tuttle, J.D., Ahijevych, D.A. and Trier, S.B. (2002) Inferences of Predictability Associated with Warm Season Precipitation Episodes. *Journal of the Atmospheric Sciences*, **59**, 2033-2056. https://doi.org/10.1175/1520-0469(2002)059<2033:IOPAWW>2.0.CO;2

[31] Laing, A.G., Carbone, R., Levizzani, V. and Tuttle, J. (2008) The Propagation and Diurnal Cycle of Deep Convection in Northern Tropical Africa. *Quarterly Journal of the Royal Meteorological Society*, **134**, 93-109. https://doi.org/10.1002/qj.194

[32] Vegunopal, V., Virts, K., Sukhatme, J., Wallace, J.M. and Chattopadhyay, B. (2015) A Comparison of the Fine-Scale Structure of the Diurnal Cycle of Tropical Rain and Lightning. *Atmospheric Research*, **169**, 515-522. https://doi.org/10.1016/j.atmosres.2015.09.004

[33] Rudlosky, S.D. and Shea, D.T. (2013) Evaluating WWLLN Performance Relative to TRMM/LIS. *Geophysical Research Letters*, **40**, 2344-2349. https://doi.org/10.1002/grl.50428

[34] Laing, A.G., Carbone, R.E. and Levizzani, V. (2011) Cycles and Propagation of Deep Convection over Equatorial Africa. *Monthly Weather Review*, **139**, 2832-2853.

https://doi.org/10.1175/2011MWR3500.1

[35] Peixoto, J.P. and Oort, A.H. (1992) Physics of Climate. American Institute of Physics, College Park, 520 p.

[36] Diaz, M. and Aiyyer, A. (2013) The Genesis of African Easterly Waves by Upstream Development. *Journal of the Atmospheric Sciences*, **70**, 3492-3512. https://doi.org/10.1175/JAS-D-12-0342.1

[37] Alaka, G.J. and Maloney, E.D. (2014) The Intraseasonal Variability of African Easterly Wave Energetics. *Journal of Climate*, **27**, 6559-6580. https://doi.org/10.1175/JCLI-D-14-00146.1

[38] Li, Y., Li, J., Jin, F.F. and Zhao, S. (2015) Interhemispheric Propagation of Stationary Rossby Waves in a Horizontally Nonuniform Background Flow. *Journal of the Atmospheric Sciences*, **72**, 3233-3256. https://doi.org/10.1175/JAS-D-14-0239.1

[39] Sinclaire, Z., Lenouo, A., Tchawoua, C. and Janicot, S. (2015) Synoptic Kelvin Type Perturbation Waves over Congo Basin over the Period 1979-2010. *Journal of Atmospheric and Solar-Terrestrial Physics*, **130**-**131**, 43-56. https://doi.org/10.1016/j.jastp.2015.04.015

[40] Wang, B. (2002) Kelvin Waves. Elsevier Science Ltd., Amsterdam, 7 p. http://www.soest.hawaii.edu

[41] Kiladis, G.N., Wheeler, M.C., Haertel, P.T., Straub, K.H. and Roundy, P.E. (2009) Convectively Coupled Equatorial Waves. *Reviews of Geophysics*, **47**, 1-42. https://doi.org/10.1029/2008RG000266

[42] King, M.J., Wheeler, C.M. and Lane, P.T. (2015) Association of Convection with the 5-Day Rossby-Haurwitz Wave. *Journal of the Atmospheric Sciences*, **72**, 3309-3321. https://doi.org/10.1175/JAS-D-14-0316.1

[43] Berhane, F., Zaitchik, B. and Badr, H.S. (2015) The Madden-Julian Oscillation's Influence on Spring Rainy Season Precipitation over Equatorial West Africa. *Journal of Climate*, **28**, 8653-8672. https://doi.org/10.1175/JCLI-D-14-00510.1

[44] Lenouo, A., Sall, S.M., Badiane, D., Gaye and Mkankam, F.K. (2016) Intense Convection over West Africa during AMMA SOP3 Experiment. *Atmospheric Research*, **180**, 1-11. https://doi.org/10.1016/j.atmosres.2016.05.002